Surfaces and Interfaces 34 (2022) 102313

Contents lists available at ScienceDirect

Surfaces and Interfaces

journal homepage: www.sciencedirect.com/journal/surfaces-and-interfaces

Atmospheric flash annealing of low-dimensional vanadium nanolayers sputtered on glass substrates

A.J. Santos [a,b,c,*], N. Martin [c], J. Outón [a,d], A. Casas-Acuña [a,b,d], E. Blanco [a,d], R. García [a,b], F. M. Morales [a,b]

[a] IMEYMAT: Institute of Research on Electron Microscopy and Materials of the University of Cádiz, Spain
[b] Department of Materials Science and Metallurgic Engineering, and Inorganic Chemistry, Faculty of Sciences, University of Cádiz, Spain
[c] Institut FEMTO-ST, UMR 6174 CNRS, Université Bourgogne Franche-Comté, 15B, Avenue des montboucons, Besançon Cedex 25030, France
[d] Department of Condensed Matter Physics, Faculty of Sciences, University of Cádiz, 11510 Puerto Real, Cádiz, Spain

ARTICLE INFO

Keywords:
Vanadium dioxide
Low-dimensional thin films
Atmospheric flash annealing
Thermochromic coatings
Low transition temperature
Smart windows

ABSTRACT

A simple approach to attain low-dimensional, highly transparent VO_2-based thermochromic coatings on glass substrates is reported. This two-step procedure comprises the initial deposition of DC magnetron-sputtered vanadium films and the subsequent flash annealing of such layers in air atmosphere. The careful control of the thermal treatment parameters and characterizations carried out by scanning electron microscopy and variable temperature Vis-NIR spectrophotometry allowed the optimization of VO_2 yields for 12.5 nm and 25 nm thick layers. The impact of layer thickness and the nature of the thermal treatment itself on the thermochromic features of such systems were also evaluated. In this sense, the resulting systems developed asymmetric transmittance vs. temperature hysteresis loops as well as a surprisingly advantageous lowering of the phase transition temperature, which is achieved without the incorporation of dopants. The most promising results were obtained for a 12.5 nm thick layer flash annealed at 475 °C, which, despite having a moderate solar modulation ability (~2%), could be a potential candidate for smart windows applications given its high Vis-NIR transparency (> 60%) coupled with its low transition temperature of 16 °C below the standard value for pure VO_2.

1. Introduction

Vanadium dioxide (VO_2) has attracted the attention of the scientific community since it undergoes a first order phase transition from the insulating monoclinic (M1) phase to the rutile (R) metallic phase at around 68 °C [1–4]. This metal-to-insulator transition (MIT) is accompanied by substantial changes in electrical resistivity and infrared optical transmittance, making this material a perfect candidate for a large number of applications such as sensors [5], resistive and THz switching [6,7], or thermochromic smart windows [8–11]. However, the large-scale transfer of this technology has been limited by the complexity and high cost of conventional VO_2 synthesis routes, either as thin films [12–15] or as nanoparticles [16–18]. This, in turn, is closely related to the complex chemistry of vanadium [19–21]: existence of other more thermodynamically stable oxides such as V_2O_5, different metastable polymorphs of VO_2, etc.

Recently, new approaches based on the atmospheric oxidation of metallic vanadium have emerged as a simple and cost-effective alternative for obtaining VO_2 [22–26]. In this regard, several studies have dealt with the air oxidation of magnetron sputtered vanadium thin films on sapphire substrates [27,28]. However, neither the substrate employed nor the thicknesses addressed (> 50 nm) were the most appropriate for optical applications in smart windows. In this paper, we report on the fabrication of low-dimensional VO_2-based thermochromic coatings by the atmospheric flash annealing oxidation of metallic vanadium films deposited on glass substrates.

2. Materials and methods

Films were deposited at room temperature by DC magnetron sputtering from a vanadium metallic target (51 mm diameter and 99.9 atomic% purity) in a homemade deposition chamber. It was evacuated down to 10^{-5} Pa before each run by means of a turbomolecular pump backed by a primary pump. The target was sputtered with a constant current density $J = 100$ A m^{-2}. Glass substrates (Menzel Gläser ® microscope slides) were placed at 65 mm from the target center. Argon was

* Corresponding author at: IMEYMAT: Institute of Research on Electron Microscopy and Materials of the University of Cádiz, Spain.
E-mail address: antonio.santos@uca.es (A.J. Santos).

https://doi.org/10.1016/j.surfin.2022.102313
Received 11 July 2022; Received in revised form 12 August 2022; Accepted 27 August 2022
Available online 31 August 2022

injected at a mass flow rate of 2.40 sccm and the pumping speed was maintained at $S = 13.5$ L s^{-1} leading to a sputtering pressure of 0.3 Pa. The deposition time was adjusted in order to obtain vanadium film thicknesses of 12.5 and 25 nm.

After deposition, vanadium samples were thermally treated in a homemade reaction system consisting in an Al_2O_3 tube on a SiC resistors furnace being able to reach 1500 °C, with an attached concentric steel tube where a high-temperature steel covered K-type thermocouple inside which acts as an axle for a system of horizontal translation. At the end of the metallic tube nearby the furnace, the thermocouple crosses and fixes to a cylinder placed inside this tube, mechanized with a hitch to hang a combustion boat. Thus, the thermometer tip is always placed some millimeters over the center of this alumina crucible, allowing the temperature in the reaction zone to be life-tracked. The other end side also crosses and is fixed to another piece that is part of a handlebar used to slide the specimen holders inside and outside. In this way, by fixing a temperature in the center of the furnace, one is able to control the temperature increase (heating rate) by moving the boat more and more inside the furnace. Consequently, translation routines were prepared for reaching an average heating rate of 42 °C s^{-1}, as well as for adjusting longer or shorter reaction times at a desired temperature. Lastly, all the samples were cooled down in air atmosphere.

Plan-view scanning electron microscopy (SEM) images were acquired using a FEI Nova NanoSEM operating at 5 kV in order to examine the general surface morphology of the films before and after each thermal treatment. The thermochromic optical behavior of the prepared VO_2 coatings was determined via transmission spectroscopy using an Agilent Cary 5000 spectrophotometer equipped with a custom-made temperature controlled stage. Thus, Vis-NIR transmission spectra of 380–2500 nm were recorded at selected temperatures in the range of 25–90 °C. Additionally, for the dynamic monitoring of the thermally induced phase transition, the temperature evolution of the optical transmittance at a selected NIR wavelength (2000 nm) was observed in both heating and cooling cycles at a controlled rate of 5 °C min^{-1}.

3. Results and discussion

Vanadium layers of 12.5 and 25 nm nominal thickness were flash annealed in a homemade tubular reactor that allows a precise control of the oxidation parameters. In this way, samples were rapidly heated at 42 °C s^{-1}, with variation of the pairs of maximum constant reaction temperatures (T_r) and times (t_r), followed by subsequent instantaneous cooling in air. All thermally treated samples are listed in Table 1. Note that, although t_r is always $\leq$ 5 s, the temperature requirements vary significantly depending on the volume of material to be oxidized, so that, for the same reaction time, larger vanadium thicknesses require higher T_r values.

The surface microstructures of the resulting samples were then investigated by SEM. Fig. 1 shows the top views of several annealed samples of 25 and 12.5 nm vanadium layer thickness, revealing, in both cases, the formation of granular structures. These micrographs also disclose the effect of reaction times and temperatures on the development of such architectures. Although, in general, the increase of both parameters leads to larger grains, t_r gives rise to a consolidation of the former microstructure (see the example of samples T25_525_1 and T25_525_5), while T_r promotes the formation of dendritic structures with grains growing preferentially along an axial direction (sample T25_575_1). On the other hand, no significant differences were found between the surface microstructure of samples with different thicknesses treated under the same conditions (i.e., T25_525_1 vs. T12.5_525). This leads us to think that this characteristic is not affected by the total volume of the material to be oxidized. However, this does not imply that these two samples have similar optical behaviors.

Table 1
Plateau conditions and thickness of V overlayers for the samples thermally treated in this study.

Sample	Thickness (nm)	Tr (°C)	tr (s)
T25_525_1	25	525	1
T25_525_5			5
T25_550_1		550	1
T25_550_5			5
T25_575_1		575	1
T12.5_450	12.5	450	1
T12.5_475		475	
T12.5_500		500	
T12.5_525		525	

T_r is the maximum reaction temperature and t_r is the reaction time.

Fig. 2 displays the Vis-NIR transmittance spectra (380–2500 nm) at 25 °C and 90 °C for all the flash annealed samples. Overall, an improvement in transmittance is observed as the thickness of the coating decreases. This is also confirmed by the parameters that assess the suitability of these systems for smart windows applications, which are listed in Table 2: (i) the luminous transmittance, T_{lum}; (ii) the solar modulation ability, ΔT_{sol}; and (iii) the solar modulation in the near infrared, ΔT_{IR}. The combined analysis of all the outcomes obtained through the optical characterization allow us to evaluate and identify the different mixtures of vanadium oxides achieved as a function of the reaction conditions (T_r and t_r) and the film thickness.

Firstly, the results obtained for the 25 nm samples (Fig. 2(a)) reveal the existence of an optimal thermal treatment gap for a temperature range between 525 °C and 575 °C. Similarly, it was also found that the optimal reaction times decrease from 5 to 1 s as the temperature increases within the previously defined range. Furthermore, based on the approaches developed in previous studies [23,24], it might be said that the optimal samples are mainly composed of VO_2 coexisting with minority mixtures of VO_x and/or VO_y, with $x < 2$ and $y > 2$, respectively. On the contrary, thermal treatments below and above the defined optimal intervals give rise to a depletion of the VO_2 yields, with mixtures enriched in VO_x (T25_525_1, characterized by lower visible transmittances) and VO_y (T25_550_5, presenting visible transmittances considerably higher than in the NIR range), respectively. The photometric parameters calculated for the optimal samples reveal moderate T_{lum} values (40–51%), which suggest that higher layer thicknesses can only lead to a drop in these values. In other words, layer thicknesses greater than 25 nm would lead to the attainment of thermochromic systems provided with insufficient visible transmittance for application in smart glasses, which require T_{lum} values above 60%. Slight variations were also observed between the T_{lum} values obtained at 25 °C and 90 °C for the optimal samples ($\Delta T_{lum} \leq 1\%$), which is a characteristic feature of flash annealing [23,24]. With regard to the information provided by the radiometric parameters, it should be noted that the optimum samples present fairly similar thermochromic behaviors ($\Delta T_{sol,\ rel}$ = 4.7–6.2%; $\Delta T_{IR,\ rel}$ = 12–14%), highlighting the slightly higher values registered for sample T25_575_1, which is associated with a higher VO_2 content. This is supported by the lower T_{lum} values reported for this sample, which is explained by an enrichment of the low visible transmittance VO_2 phase (antagonistic relationship between T_{lum} and ΔT_{sol} [29]). In any case, the solar modulation ability of the optimal 25 nm thick VO_2-based systems is rather modest ($\Delta T_{sol} < 2.3\%$).

On the other hand, Fig. 2(b) shows the Vis-NIR transmittance spectra recorded for 12.5 nm thick samples subjected to flash annealing, also revealing a progressive evolution of VO_x-VO_2-VO_y combinations as the reaction temperature increases from 475 °C (mostly VO_x) to 525 °C (VO_y mixtures). As mentioned above, the decrease in layer thickness results in higher visible transmittances (T_{lum} values between 55 and 70%). However, this fact translates into a generalized decrease of ΔT_{sol} and ΔT_{IR} values (Table 2). Thus, it is evidenced that thicknesses below 25 nm lead to a decrease in solar modulation capacity (lower VO_2 vol), which in turn explains the higher transmittance of these coatings. Nevertheless, thicknesses below 12.5 nm would seriously compromise the thermochromic response of these systems, limiting their application. With this

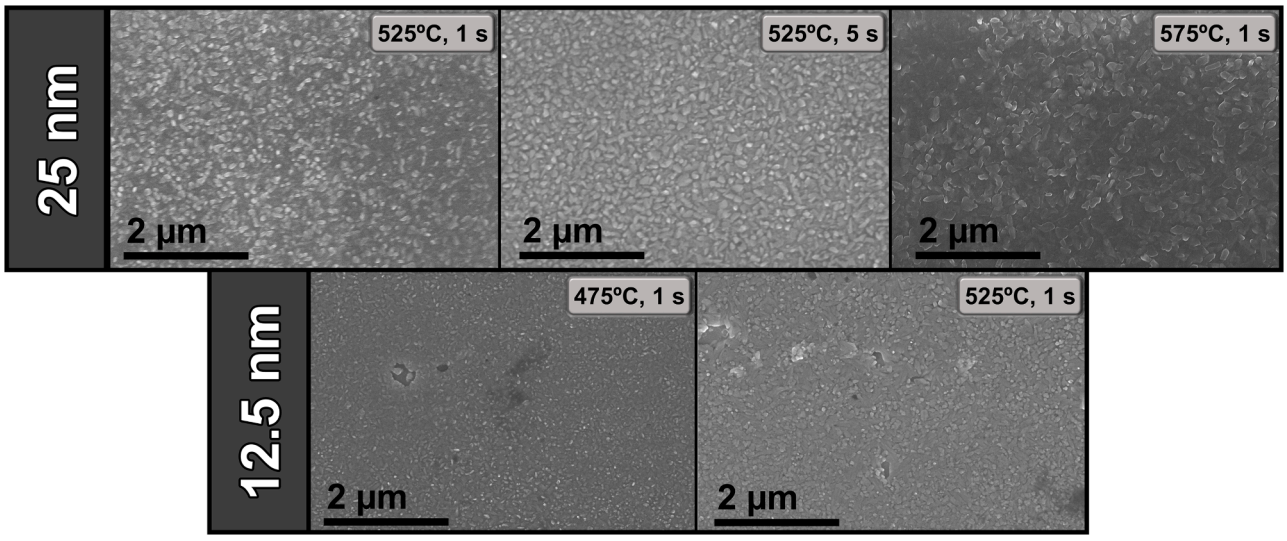

Fig. 1. SEM planar view of 25 and 12.5 nm samples subjected to different reaction temperatures (T_r) and times (t_r), as labelled in the images.

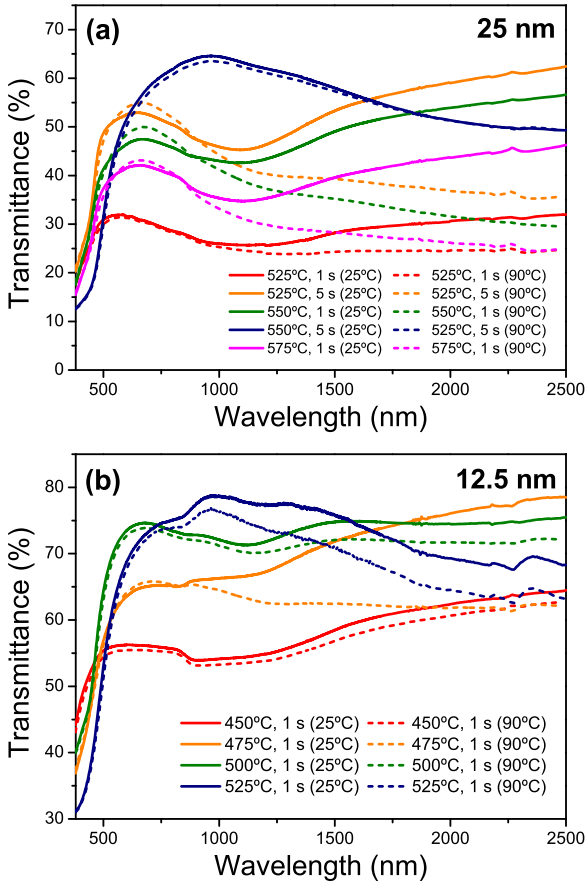

Fig. 2. Transmittance spectra recorded at 25 °C (solid lines) and 90 °C (dashed lines) for (a) 25 nm and (b) 12.5 nm thick samples oxidized at different temperatures (T_r = 450–575 °C) and times (t_r = 1–5 s).

in mind, the samples that achieved the best compromise between T_{lum} and ΔT_{sol} values were T12.5_475 and T12.5_525. However, although both samples exhibit very similar values for both parameters, their physicochemical characteristics are quite different. On one side, the signatures of their transmittance spectra suggest that sample T12.5_475 would consist mainly of VO_2 (coexisting with minority fractions of VO_x and/or VO_y), whereas sample T12.5_525 would be composed of VO_2 + VO_y mixtures. This is in fine agreement with the relative near-infrared solar modulation values ($\Delta T_{IR,\ rel}$) calculated for these two optimal samples ($\Delta T_{IR,\ rel}$ = 6.6% and 4.0% for T12.5_475 and T12.5_525, respectively). Nonetheless, the most remarkable difference between the parameters calculated for these samples comes from the variations in luminous transmittance (ΔT_{lum}), being significantly higher for T12.5_525 (ΔT_{lum} = 1.3%). This phenomenon, which has been previously observed in $VO_2 + VO_y$ mixtures [23,24,31,32], would explain the ΔT_{sol} value obtained for sample T12.5_525 even though it has less VO_2 than T12.5_475, finding its origin in an additional solar modulation at 400–1000 nm (the window of the electromagnetic spectrum in which solar irradiance becomes maximum).

Table 2
Radiometric (T_{sol}) and photometric (T_{lum}) parameters changes with heating for all the studied samples.

Sample	T_{lum} (%)	ΔT_{lum} (%)	ΔT_{sol} (%)	$\Delta T_{sol.\ rel}$ (%)	ΔT_{IR} (%)	$\Delta T_{IR.\ rel}$ (%)
T25_525_1	31.2	0.6	1.1	3.9	1.9	6.9
T25_525_5	51.1	0.4	2.2	4.7	6.1	12.2
T25_550_1	44.9	1.0	2.1	4.9	6.1	13.3
T25_550_5	43.9	1.6	1.0	2.0	0.9	1.4
T25_575_1	39.9	0.0	2.3	6.2	5.4	14.2
T12.5_450	55.5	0.8	0.9	1.7	1.0	1.9
T12.5_475	61.2	0.1	1.8	2.9	4.5	6.6
T12.5_500	69.8	0.9	1.1	1.6	1.5	2.0
T12.5_525	62.5	1.3	1.9	2.9	3.0	4.0

For a detailed definition and explanation of how all these parameters are obtained, refer to the work of Outón et al. (Appendix A) [30].

The main features of the metal-to-insulator hysteresis were examined from the kinetic evolution of transmittance at 2000 nm in heating and cooling cycles at a constant rate (Fig. 3). The samples that showed the best optical responses were investigated: (i) T12.5_475, which, at equal T_{lum} and ΔT_{sol} values, was selected over the T12.5_525 for exhibiting a most stable optical behavior at visible wavelengths; and (ii) T25_550_1, which presents intermediate characteristics to those samples achieved at temperatures and reaction times located at both extremes of the optimal thermal treatment windows for 25 nm films. Complementarily, Table 3 lists the transition temperatures, for heating ($T_{c(H)}$) and cooling ($T_{c(C)}$) cycles. They are calculated from the derivative curves of the transmittance plots (Fig. 3(a)) with a Gaussian fit (see Fig. 3(b–c)), along with the hysteresis loop width (W_H), transmittance at 2000 nm for 25 °C (T_{max}) and for 90 °C (T_{min}), and their relative difference.

As can be seen in Fig. 3, both samples are characterized by the

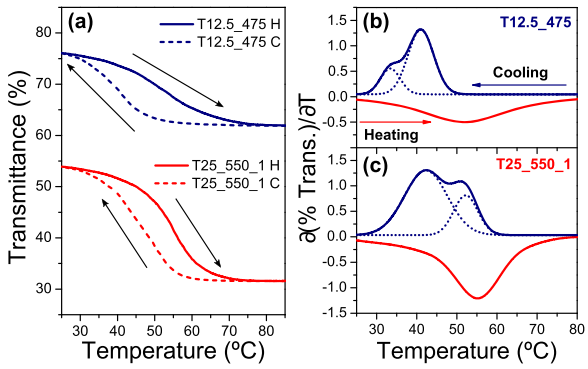

Fig. 3. (a) Thermal evolution of the optical transmittance at 2000 nm of T12.5_475 (blue) and T25_550_1 (red) samples for consecutive heating (solid lines) and cooling (dashed lines) cycles. Derivative of each kinetic thermochromic cycle for samples (b) T12.5_475 and (c) T25_550_1 for heating (red) and cooling (blue). For a better overview, the derivatives of the cooling are plotted in absolute values. (For interpretation of the references to colour in this figure legend, the reader is referred to the web version of this article.)

this study, which are expected to contain significant V_2O_5 fractions (most thermodynamically stable phase within the VO_y oxides). The latter, in turn, would considerably enhance the durability of these thermochromic coatings, so that V_2O_5 would act as a protective overlayer for VO_2 against external agents such as air or humidity [38,39]. This agrees with our previous study [26], which evidenced that the atmospheric rapid annealing of vanadium thin films results the in development of gradient of phases from V_2O_5 to V_2O_3, with an intermediate VO_2 region, from the surface to the interface with the substrate. Further, the action of the effects described above results in the appearance of a variable hysteresis width of 11–19 °C.

Conversely, the hysteresis loop of sample T25_550_1 also presents two slopes during the cooling stage, although, in contrast to the previous observations for T12.5_475, the second slope is slightly steeper than the first one, suggesting the presence of larger amounts of the metastable VO_2(M2) phase. It seems that the promotion of this polymorph could be further favored either by increasing layer thickness or reaction temperature (larger grains). Furthermore, although still much lower than those reported for pure VO_2, the T_c values registered for sample T25_550_1 during the heating-cooling cycles were found to be higher

Table 3
Main features of the thermochromic hysteresis loops illustrated in Fig. 3.

Sample	$T_{c(H)}$ (°C) heating	$T_{c(C)}$ (°C) cooling		W_H (°C)		T_{max} (%)	T_{min} (%)	ΔT_{rel} (%)
		C1	C2	1	2			
T12.5_475	52	41*	33	11	19	76.1	61.9	18.6
T25_550_1	55	52	42*	3	13	53.9	31.6	41.4

* Main peak.

$T_{c(H)}$ denotes the temperatures of the MIT transition on heating; $T_{c(C1)}$ and $T_{c(C2)}$ indicate the temperatures of the MIT on cooling. W_{H1} and W_{H2} are the hysteresis loop widths given by $T_{c(H)} - T_{c(C1)}$ and $T_{c(H)} - T_{c(C2)}$, respectively. T_{max}, and T_{min} denote the 2000 nm wavelength transmittances at 25 °C and 90 °C, respectively. ΔT_{rel} is the relative decrease of transmittance upon the transition at 2000 nm.

development of asymmetric hysteresis loops during the cooling cycles, as well as the shift of the transition temperatures towards lower values, which is achieved without doping. First, we will focus on the particularities of sample T12.5_475. Fig. 3(b) reveals two different slopes (the first one steeper; the second one more gradual) during cooling cycles, giving rise to minimum variation rates (absolute minimum of the optical hysteresis derivatives) at $T_{c(C1)} = 41$ °C and $T_{c(C2)} = 33$ °C. Although it differs from what has been previously observed for the flash annealing of porous vanadium films [23,24], this is an intrinsic feature of rapid thermal treatments, which is explained by the coexistence of VO_2(M1) with the metastable VO_2(M2) phase [33]. In contrast, the heating cycles lead to a single transition temperature that is considerably lower ($T_{c(H)} = 52$ °C) than those reported for pure VO_2 films (~68 °C). In any case, it is worth mentioning that the transition temperatures recorded during the heating-cooling cycles are both low, which has been previously associated with the presence of oxygen-deficiency-related defects [34,35]. This remarkable phenomenon, actually beneficial for smart glazing applications, would be favored by the flash annealing treatments addressed here, so that oxidation takes place so rapidly that the stoichiometry $O/V = 2$ cannot be completely reached. Notwithstanding, it seems that there is a lack of consensus on the origin and mechanism behind the reduction of T_c values without the incorporation of dopants. Alternatively, several authors have attributed this event to the presence of a residual tensile stress near the film-substrate interface [36–38], which gradually weakens with increasing thickness (i.e. lower thicknesses lead to higher T_c drops). Others, however, have associated it with the internal compressive stress originated due to mismatch shrinkage between VO_2(M) and V_2O_5 during the cooling stage which forces a shorter V–V bond in VO_2(M), leading to an easier transition from VO_2(M) to VO_2(R) [39]. Note that all of the above assumptions could fully or partially explain the decrease in T_c for the systems addressed in

than those obtained for sample T12.5_475. This is in line with our previous hypothesis that the drops in T_c are due to the combined effect of oxygen substoichiometry, the presence of V_2O_5, and the decrease in layer thickness. Likewise, thicker films, while also resulting in variable W_H (Table 3), lead to narrower hysteresis loops, which is in agreement with what has been previously reported in the literature [37,40]. Apart from that, the confrontation of the ΔT_{rel} values obtained for both

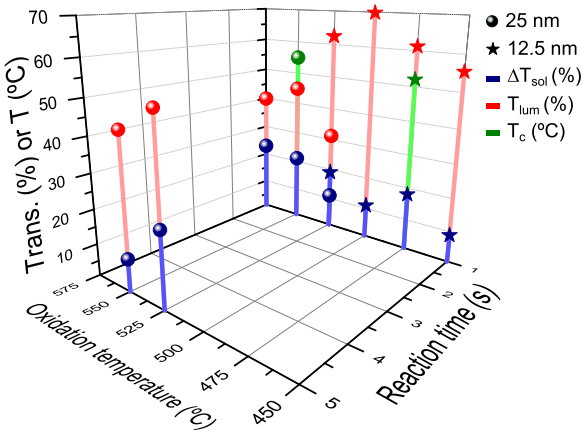

Fig. 4. Summary of the thermochromic performances achieved for oxidized 25 and 12.5 nm thick films (ΔT_{sol}, T_{lum}, and T_c) as a function of oxidation temperature (T_r) and reaction time (t_r). The transition temperature T_c values referred here correspond to those extracted from the heating cycles ($T_{c(H)}$). The z-axis returns simultaneously the percentage of transmittance (ΔT_{sol} and T_{lum} outputs) as well as the temperature (T_c outputs). Also note that, for a better overview, ΔT_{sol} values were plotted multiplied by a factor of 10.

samples highlights a higher VO_2 vol for sample T25_550_1, which is closely linked to its greater layer thickness.

Fig. 4 illustrates the overall results obtained for all flash annealed samples based on the values of the parameters that determine their thermochromic performance for smart window applications as a function of layer thickness as well as reaction temperatures and times. As can be seen, 12.5 nm thick samples offer considerably higher visible transmittance than those obtained from 25 nm samples. On the contrary, even though the latter have a higher ability to modulate solar irradiance, the ΔT_{sol} values obtained for all the samples studied are quite moderate for practical applications in smart windows (ΔT_{sol} values greater than 5% are generally required). In any case, these results fail to match and/or improve those achieved by the flash annealing of vanadium films deposited at glancing angles (V-GLAD) [23,24], emphasizing the positive effect of the inclusion of porosity on the substantial improvement of reactivity and selectivity for VO_2(M1) synthesis. Despite this, the outcomes obtained for sample T12.5_475 are quite significant, reaching rather good T_{lum} values (> 60%) at the same time as a T_c drop of 16 °C lower than those reported for undoped VO_2 films. This becomes even more relevant given the simplicity and advantages of the synthesis strategy addressed in this work (fast sputtering plus a quick oxidation in air atmosphere without additional requirements such as the presence of catalysts, reactive gasses, vacuum, long-time processing, etc.). Furthermore, the high transparency recorded for the T12.5_475 and T25_525_5 samples in the NIR region, coupled with a decent thermochromic response, makes them at the same time potential candidates for certain IR applications (sensors, detectors,…) [41].

4. Conclusions

In conclusion, it has been shown that air-atmosphere flash annealing of low-dimensional vanadium films sputtered on glass substrates leads to the synthesis of thermochromic VO_x-VO_2-VO_y ($x < 2$; $y > 2$) layers exhibiting T_c values 13–16 °C below those reported for undoped samples. This phenomenon is attributed to the combined effect of oxygen deficiency (a direct consequence of instantaneous oxidation), the presence of V_2O_5, and the very narrow layer thicknesses addressed in this study. Likewise, it is estimated that the flash annealing of vanadium thicknesses below 12.5 nm and above 25 nm would result in a considerable depletion of the luminous transmittance (T_{lum}) and solar modulation capacity (ΔT_{sol}), respectively. These thermal treatments also appear to promote the formation of significant amounts of the VO_2(M2) polymorph. By simply adjusting the reaction times and oxidation temperatures for a given vanadium layer thickness, the VO_2 yields were optimized. However, the ΔT_{sol} values accomplished were rather discrete (around 2%) compared to those obtained by the flash annealing of V-GLAD layers (improved reactivity and selectivity for VO_2 synthesis). The most remarkable results for smart window applications were obtained for the 12.5 nm thick sample instantaneously oxidized ($t_r = 1$ s) at 475 °C, which presented a T_{lum} value above 60%, a high transparency in the NIR range (70% on average), and an extraordinarily low transition temperature without doping ($T_{c(H)} = 52$ °C).

CRediT authorship contribution statement

A.J. Santos: Conceptualization, Methodology, Validation, Formal analysis, Investigation, Data curation, Writing – original draft, Writing – review & editing, Visualization, Project administration, Funding acquisition. **N. Martin:** Conceptualization, Methodology, Investigation, Resources, Writing – review & editing, Supervision, Project administration, Funding acquisition. **J. Outón:** Formal analysis, Investigation. **A. Casas-Acuña:** Investigation. **E. Blanco:** Resources. **R. García:** Resources, Supervision. **F.M. Morales:** Conceptualization, Methodology, Validation, Formal analysis, Resources, Writing – review & editing, Supervision, Project administration, Funding acquisition.

Declaration of Competing Interest

The authors declare that they have no known competing financial interests or personal relationships that could have appeared to influence the work reported in this paper.

Acknowledgments

A. J. Santos would like to thank the University of Cádiz and the Spanish Ministerio de Universidades for the concession of a "Margarita Salas" postdoctoral fellowship funded by the European Union - NextGenerationEU (sol-202100211960-tra). J. Outón acknowledges the support by the Spanish Ministerio de Educación y Cultura through grant FPU19–02638. University of Cádiz and IMEYMAT are also acknowledged by financing the mutual facilities available at the UCA R&D Central Services (SC-ICYT), the UCA project references "PUENTE PR2020–003″ and "OTRI AT2019/032″, and the IMEYMAT project reference "LÍNEAS PRIORITARIAS PLP2021120–1″. This work was supported by the Spanish State R&D project (Retos y Generación de Conocimiento) ref. PID2020–114418RBI00. The regional government of Andalusia with FEDER co-funding also participates through the projects AT-5983 Trewa 1157178 and FEDER-UCA18–10788. This work was partly supported by the french RENATECH network, FEMTO-ST technological facility, by the Region Bourgogne-Franche-Comté and by EIPHI Graduate School (Contract "ANR–17–EURE–0002″).

Data availability statement

The raw/processed data required to reproduce these findings cannot be shared at this time due to technical or time limitations.

References

[1] J.B. Goodenough, The two components of the crystallographic transition in VO_2, J. Solid State Chem. 3 (1971) 490–500, https://doi.org/10.1016/0022-4596(71)90091-0.
[2] V. Devthade, S. Lee, Synthesis of vanadium dioxide thin films and nanostructures, J. Appl. Phys. 128 (2020), 231101, https://doi.org/10.1063/5.0027690.
[3] S. Wang, M. Liu, L. Kong, Y. Long, X. Jiang, A. Yu, Recent progress in VO_2 smart coatings: strategies to improve the thermochromic properties, Prog. Mater. Sci. 81 (2016) 1–54, https://doi.org/10.1016/j.pmatsci.2016.03.001.
[4] K. Liu, S. Lee, S. Yang, O. Delaire, J. Wu, Recent progresses on physics and applications of vanadium dioxide, Mater. Today 21 (2018) 875–896, https://doi.org/10.1016/j.mattod.2018.03.029.
[5] E. Strelcov, Y. Lilach, A. Kolmakov, Gas sensor based on metal-insulator transition in VO_2 nanowire thermistor, Nano Lett. 9 (2009) 2322–2326, https://doi.org/10.1021/nl900676n.
[6] N. Émond, A. Hendaoui, A. Ibrahim, I. Al-Naib, T. Ozaki, M. Chaker, Transmission of reactive pulsed laser deposited VO_2 films in the THz domain, Appl. Surf. Sci. 379 (2016) 377–383, https://doi.org/10.1016/j.apsusc.2016.04.018.
[7] J. del Valle, P. Salev, F. Tesler, N.M. Vargas, Y. Kalcheim, P. Wang, J. Trastoy, M. H. Lee, G. Kassabian, J.G. Ramírez, M.J. Rozenberg, I.K. Schuller, Subthreshold firing in Mott nanodevices, Nature 569 (2019) 388–392, https://doi.org/10.1038/s41586-019-1159-6.
[8] Y. Cui, Y. Ke, C. Liu, Z. Chen, N. Wang, L. Zhang, Y. Zhou, S. Wang, Y. Gao, Y. Long, Thermochromic VO_2 for energy-efficient smart windows, Joule 2 (2018) 1707–1746, https://doi.org/10.1016/j.joule.2018.06.018.
[9] T.C. Chang, X. Cao, S.H. Bao, S.D. Ji, H.J. Luo, P. Jin, Review on thermochromic vanadium dioxide based smart coatings: from lab to commercial application, Adv. Manuf. 6 (2018) 1–19, https://doi.org/10.1007/s40436-017-0209-2.
[10] N. Shen, S. Chen, R. Huang, J. Huang, J. Li, R. Shi, S. Niu, A. Amini, C. Cheng, Vanadium dioxide for thermochromic smart windows in ambient conditions, Mater. Today Energy 21 (2021), 100827, https://doi.org/10.1016/j.mtener.2021.100827.
[11] X. Cao, T. Chang, Z. Shao, F. Xu, H. Luo, P. Jin, Challenges and opportunities toward real application of VO_2-based smart glazing, Matter. 2 (2020) 862–881, https://doi.org/10.1016/j.matt.2020.02.009.
[12] M.M. Seyfouri, R. Binions, Sol-gel approaches to thermochromic vanadium dioxide coating for smart glazing application, Sol. Energy Mater. Sol. Cells 159 (2017) 52–65, https://doi.org/10.1016/j.solmat.2016.08.035.
[13] Y.L. Wang, X.K. Chen, M.C. Li, R. Wang, G. Wu, J.P. Yang, W.H. Han, S.Z. Cao, L. C. Zhao, Phase composition and valence of pulsed laser deposited vanadium oxide thin films at different oxygen pressures, Surf. Coat. Technol. 201 (2007) 5344–5347, https://doi.org/10.1016/j.surfcoat.2006.07.087.
[14] J. Du, Y. Gao, H. Luo, L. Kang, Z. Zhang, Z. Chen, C. Cao, Significant changes in phase-transition hysteresis for Ti-doped VO_2 films prepared by polymer-assisted

deposition, Sol. Energy Mater. Sol. Cells 95 (2011) 469–475, https://doi.org/10.1016/j.solmat.2010.08.035.
[15] R. Binions, G. Hyett, C. Piccirillo, I.P. Parkin, Doped and un-doped vanadium dioxide thin films prepared by atmospheric pressure chemical vapour deposition from vanadyl acetylacetonate and tungsten hexachloride: the effects of thickness and crystallographic orientation on thermochromic properties, J. Mater. Chem. 17 (2007) 4652–4660, https://doi.org/10.1039/b708856f.
[16] G. Bragaggia, A. Cacciatore, E. Poffe, C. Capone, F. Zorzi, V. Causin, S. Gross, Systematic exploration of the synthetic parameters for the production of dynamic VO_2(M1), Molecules 26 (2021) 4513, https://doi.org/10.3390/molecules26154513.
[17] N. Shen, B. Dong, C. Cao, Z. Chen, H. Luo, Y. Gao, Solid-state-reaction synthesis of VO_2 nanoparticles with low phase transition temperature, enhanced chemical stability and excellent thermochromic properties, RSC Adv. 5 (2015) 108015–108022, https://doi.org/10.1039/c5ra20732k.
[18] J. Qi, G. Ning, Y. Lin, Synthesis, characterization, and thermodynamic parameters of vanadium dioxide, Mater. Res. Bull. 43 (2008) 2300–2307, https://doi.org/10.1016/j.materresbull.2007.08.016.
[19] A. Perucchi, L. Baldassarre, P. Postorino, S. Lupi, Optical properties across the insulator to metal transitions in vanadium oxide compounds, J. Phys. Condens. Matter. 21 (2009), 323202, https://doi.org/10.1088/0953-8984/21/32/323202.
[20] M.G. Krishna, Y. Debauge, A.K. Bhattacharya, X-ray photoelectron spectroscopy and spectral transmittance study of stoichiometry in sputtered vanadium oxide films, Thin Solid Films 312 (1998) 116–122, https://doi.org/10.1016/S0040-6090(97)00717-7.
[21] E. Hryha, E. Rutqvist, L. Nyborg, Stoichiometric vanadium oxides studied by XPS, Surf. Interface Anal. 44 (2012) 1022–1025, https://doi.org/10.1002/sia.3844.
[22] F.M. Morales, M. Escanciano, M.P. Yeste, A.J. Santos, Reactivity of vanadium nanoparticles with oxygen and tungsten, Nanomaterials 12 (2022) 1471, https://doi.org/10.3390/nano12091471.
[23] A.J. Santos, N. Martin, J. Outón, E. Blanco, R. García, F.M. Morales, Towards the optimization of a simple route for the fabrication of energy-efficient VO_2-based smart coatings (under review in J Materiomics).
[24] A.J. Santos, N. Martin, J. Outón, E. Blanco, R. García, F.M. Morales, A simple two-step approach to the manufacture of VO2-based coatings with unique thermochromic features for energy-efficient smart glazing (under review in Energy Build.).
[25] A.J. Santos, M. Escanciano, A. Suárez-Llorens, M.P. Yeste, F.M. Morales, A novel route for the easy production of thermochromic VO_2 nanoparticles, Chem. Eur. J. 27 (2021) 16662–16669, https://doi.org/10.1002/chem.202102566.
[26] A.J. Santos, B. Lacroix, M. Domínguez, R. García, N. Martin, F.M. Morales, Controlled grain-size thermochromic VO_2 coatings by the fast oxidation of sputtered vanadium or vanadium oxide films deposited at glancing angles, Surf. Interfaces 27 (2021), 101581, https://doi.org/10.1016/j.surfin.2021.101581.
[27] P. Ashok, Y.S. Chauhan, A. Verma, Vanadium dioxide thin films synthesized using low thermal budget atmospheric oxidation, Thin Solid Films 706 (2020), 138003, https://doi.org/10.1016/j.tsf.2020.138003.
[28] P. Ashok, Y.S. Chauhan, A. Verma, Effect of vanadium thickness and deposition temperature on VO_2 synthesis using atmospheric pressure thermal oxidation, Thin Solid Films 724 (2021), 138630, https://doi.org/10.1016/j.tsf.2021.138630.
[29] S.Y. Li, G.A. Niklasson, C.G. Granqvist, Thermochromic fenestration with VO_2-based materials: three challenges and how they can be met, Thin Solid Films 520 (2012) 3823–3828, https://doi.org/10.1016/j.tsf.2011.10.053.
[30] J. Outón, E. Blanco, M. Domínguez, H. Bakkali, J.M. Gonzalez-Leal, J.J. Delgado, M. Ramírez-del-Solar, Tracking the optical constants of porous vanadium dioxide thin films during metal–insulator transition: influence of processing conditions on their application in smart glasses, Appl. Surf. Sci. 580 (2022), 152228, https://doi.org/10.1016/j.apsusc.2021.152228.
[31] P.L. Madhuri, S. Bhupathi, S. Shuddhodana, Z.M.A. Judeh, S.H. Yang, Y. Long, I. Abdulhalim, Hybrid vanadium dioxide-liquid crystal tunable non-reciprocal scattering metamaterial smart window for visible and infrared radiation control, Opt. Mater. Express 11 (2021) 3023–3037, https://doi.org/10.1364/OME.432784.
[32] J. Jin, D. Zhang, X. Qin, Y. Yang, Y. Huang, H. Guan, Q. He, P. Fan, W. Lv, Notable enhancement of phase transition performance and luminous transmittance in VO_2 films via simple method of Ar/O plasma post-treatment, Nanomaterials 9 (2019) 102, https://doi.org/10.3390/nano9010102.
[33] C.O.F. Ba, V. Fortin, S.T. Bah, R. Vallée, A. Pandurang, Formation of VO_2 by rapid thermal annealing and cooling of sputtered vanadium thin films, J. Vac. Sci. Technol. A. 34 (2016), 031505, https://doi.org/10.1116/1.4944606.
[34] K.L. Gurunatha, S. Sathasivam, J. Li, M. Portnoi, I.P. Parkin, I. Papakonstantinou, Combined effect of temperature induced strain and oxygen vacancy on metal-insulator transition of VO_2 colloidal particles, Adv. Funct. Mater. 30 (2020), 2005311, https://doi.org/10.1002/adfm.202005311.
[35] L. Chen, X. Wang, D. Wan, Y. Cui, B. Liu, S. Shi, H. Luo, Y. Gao, Tuning the phase transition temperature, electrical and optical properties of VO_2 by oxygen nonstoichiometry: insights from first-principles calculations, RSC Adv. 6 (2016) 73070–73082, https://doi.org/10.1039/c6ra09449j.
[36] J. Bian, M. Wang, H. Sun, H. Liu, X. Li, Y. Luo, Y. Zhang, Thickness-modulated metal–insulator transition of VO_2 film grown on sapphire substrate by MBE, J. Mater. Sci. 51 (2016) 6149–6155, https://doi.org/10.1007/s10853-016-9863-1.
[37] G. Xu, P. Jin, M. Tazawa, K. Yoshimura, Thickness dependence of optical properties of VO_2 thin films epitaxially grown on sapphire (0001), Appl. Surf. Sci. 244 (2005) 449–452, https://doi.org/10.1016/j.apsusc.2004.09.157.
[38] X. Zhou, Y. Meng, T.D. Vu, D. Gu, Y. Jiang, Q. Mu, Y. Li, B. Yao, Z. Dong, Q. Liu, Y. Long, A new strategy of nanocompositing vanadium dioxide with excellent durability, J. Mater. Chem. A 9 (2021) 15618–15628, https://doi.org/10.1039/D1TA02525B.
[39] T.D. Vu, H. Xie, S. Wang, J. Hu, X. Zeng, Y. Long, Durable vanadium dioxide with 33-year service life for smart windows applications, Mater. Today Energy 26 (2022), 100978, https://doi.org/10.1016/j.mtener.2022.100978.
[40] Y. Yang, X. Mao, Y. Yao, H. Huang, Y. Lu, L. Luo, X. Zhang, G. Yin, T. Yang, X. Gao, Thickness effects on the epitaxial strain states and phase transformations in (001)-VO_2/TiO_2 thin films, J. Appl. Phys. 125 (2019), 082508, https://doi.org/10.1063/1.5049551.
[41] M.C. Larciprete, M. Centini, S. Paoloni, I. Fratoddi, S.A. Dereshgi, K. Tang, J. Wu, K. Aydin, Adaptive tuning of infrared emission using VO_2 thin films, Sci. Rep. 10 (2020) 11544, https://doi.org/10.1038/s41598-020-68334-2.